Towards DNA unzipping with magnetic tweezers to localize nucleosomes in native chromatin

Towards DNA unzipping with magnetic tweezers to localize nucleosomes in native chromatin

Tjerk Venema

Huygens-Kamerlingh Onnes Laboratory, Leiden University
P.O. Box 9500, 2300 RA Leiden, The Netherlands

December 21, 2020

Abstract

As the basic unit of chromatin, the form in which DNA is tightly packed in the nucleus of eukaryotic cells, the nucleosome forms a physical barrier during transcription of the DNA. Understanding the energetic landscape of the nucleosome during transcription extends our knowledge on how the nucleosome affects gene expression. An *in vitro* study of the energetic landscape of native nucleosomes has never been done. To facilitate such a study, techniques need to be developed to mechanically unzip native chromatin. In this research, we developed techniques on DNA unzipping using magnetic tweezers that are needed for the localization of nucleosomes in chromatin unzipping. We investigated long-lifetime DNA tethering to improve reproducibility and experimental practicality, which is vital for tethers containing nucleosomes. Techniques of force barrier localization during DNA unzipping were developed that could be used on nucleosomes. Two-state equilibrium statistical mechanics models for DNA unzipping and overstretching were developed that are extendable to include more states. These techniques aim to facilitate experiments on native nucleosomes that shine light on their fundamental role in epigenetics.

Contents

1 Introduction

Chromatin is the form in which DNA is tightly packed in the cellular nucleus of eukaryotes. This compaction is needed to prevent entangling of the strands and to organize processes such as cell division. Chromatin is found in three levels of compaction. The nucleosome is the most basic subunit of chromatin. It consists of ~ 147 basepairs of DNA wrapped 1.7 times around a core of 8 histone proteins. Multiple nucleosomes connected by "naked" pieces of DNA create the so-called "beads-on-a-string" form of chromatin. This is the most basic form in which chromatin is found. The next level is formed by nucleosomes that stick together by use of another histone. The highest level is formed by supercoiling of chromatin together with additional packaging proteins creating chromosomes. Only DNA in a decondensed form can be accessed for transcription. This means that the expression of the genetic information encoded in the DNA, can be regulated by the dynamic structure of chromatin. The way this works is poorly understood and remains an active field of science.

It has been shown that the nucleosome forms a physical barrier during transcription of the DNA (Hodges et al., 2009; Bintu et al., 2012). The RNA polymerase II (Pol II) enzyme, responsible for transcription, is not able to actively "peel" the DNA from the histone core. Pol II only advances when the DNA fluctuates off the histone core. This suggests that the nucleosome plays a fundamental role in gene expression. However these studies were not able to map the full topography of the nucleosomal barrier during transcription. Clarifying the energetic landscape of nucleosomes during transcription is needed to understand how the nucleosome affects gene expression. Not only will this extend our knowledge on epigenetics, it is fundamental to research in diseases like cancer.

Hall et al. (2009) have made an energetic map of a nucleosome by mechanically unzipping synthetically prepared DNA containing a single nucleosome. They found three regions along the DNA sequence of strong interactions containing a ~ 5 bp periodicity, of which the middle region around the dyad of the nucleosome (center of the sequence wrapped around the histone core) was the strongest. The other two were $\sim \pm 40$ bp from the dyad. Chen et al. (2019) have made a mapping of the energy landscape of a nucleosome during transcription. They traced the Pol II enzyme along the DNA, transcribing through a single nucleosome by mechanical unzipping. They did this for two different types of nucleosomes. They observed increased dwell times of Pol II, indicating force barriers from which they were able to calculate the energy map along the nucleosome. Both studies were done using optical tweezers and synthetic DNA. The next step would be an *in vitro* study on native nucleosomes in the form of euchromatin.

Methods need to be developed to unzip native chromatin. Hermans et al. (2017) found a way to purify single genomic loci of native chromatin from cell lysate. They developed LNA probes that bind to target DNA and they developed a way to incorporate sequence-specific affinity tags to DNA. This way, a structure can be made from native chromatin on which force spectroscopy can be done. To be able to map the energetic landscape of a nucleosome, the nucleosome needs to be localized along the native sequence, because its location is unknown. This localization can be done by unzipping the chromatin. The nucleosome can then be localized by a sudden force barrier that appears during unzipping (Shundrovsky et al., 2006; Hall et al., 2009; Li and Wang, 2012). The unzipping can be performed using optical tweezers or magnetic tweezers. In optical tweezers, only one molecule can be measured at once. Magnetic tweezers on the other hand are less expensive and are relatively easy to use. Using multiplexed magnetic tweezers, more than 100 molecules can be measured individually at the same time (De Vlaminck et al., 2012;

Brouwer et al., 2020). Magnetic tweezers do have a lower nanometric resolution than optical tweezers. However, chromatin is a rather large molecule, which redeems the need for a better resolution. DNA has been unzipped using magnetic tweezers (Li et al., 2019). Unzipping nucleosomes however has never been done using magnetic tweezers.

In this research, we developed techniques for DNA unzipping that are needed for the localization of nucleosomes in chromatin unzipping. Common tethering schemes often suffer from mechanical instability resulting in short lifetimes, compromising reproducibility and experimental practicality. We therefore investigated long-lifetime DNA tethering. The tethers that were found this way, were used to learn more about DNA overstretching, which is similar in nature to unzipping. An equilibrium statistical mechanics model for DNA overstretching was developed. This overstretching model paved the way for the development of an equilibrium DNA unzipping model. Since our end goal is localizing nucleosomes along the sequence by their force barriers, techniques of localizing force barriers along the sequence were developed and tested on naked DNA. With this we prepared a foundation for the localization of nucleosomes by unzipping chromatin using magnetic tweezers.

2 Theory

2.1 DNA overstretching: equilibrium statistical mechanics model

When dsDNA is stretched from end to end with forces of $\sim 65\,\text{pN}$ and higher, the contour length of the DNA suddenly increases by $\sim 70\%$ (Smith et al., 1996; Cluzel et al., 1996). There has been much debate in the past about the structural nature of this "overstretching". Three different microscopic models arose over time: the unpeeling of one ssDNA strand from the other, where only one remains under tension; partially melted DNA, where both strands remain under tension; and an unwound ladder-like DNA structure, where base pairing remains intact, called S-DNA. Later it was shown that all three models can exist under different circumstances (King et al., 2013). The salt concentration and the topology of the DNA substrate determine which mechanism is favored. For salt concentrations below $150\,\text{mM}$ NaCl, peeling and melting is favored above S-DNA formation. The DNA twist can be free or constrained, when both strands of DNA at each end are attached to some anchoring structure connecting to the bead or the glass and there are no nicks in the DNA backbone. In this case, the DNA is not allowed to twist. When at one or both ends only one strand of DNA is attached to the anchoring structure or when there are nicks in the DNA backbone no torsional stress will build up. In such an open topology, one strand of DNA is allowed to unpeel from the other which is still held under tension. Melting bubbles can occur in an open as well as a closed topology. In a closed topology, unpeeling cannot occur.

The structure and mechanism of S-DNA is not completely understood (Zhang et al., 2012; Bongini et al., 2014; Backer et al., 2019), and beyond the scope of this work. The peeling and melting mechanisms however share similarities to DNA unzipping, which is what we are interested in. The peeling and melting mechanisms can be captured in the following equilibrium model.

DNA overstretching can be modeled as a two-macrostate system. The two macrostates will be denoted as the ds-state (B-DNA structure) and the ss-state, the overstretched state is thus interpreted as ssDNA. The force-extension relation of dsDNA is best described by an extendable worm-like chain (WLC), which is well approximated by

$$\zeta_{\text{WLC}}(F) \equiv \frac{z}{L} = 1 - \frac{1}{2}\sqrt{\frac{k_{\text{B}}T}{FA}} + \frac{F}{S}, \tag{1}$$

where z is the extension, L is the contour length of the polymer, F is the external force applied to the polymer, A is the persistence length and S is the stretch modulus (Odijk, 1995). For dsDNA, typical values of these elastic parameters are given by $A_{\text{ds}} \sim 50\,\text{nm}$ and $S_{\text{ds}} \sim 1000\,\text{pN}$. For ssDNA the force-extension relation is given by the freely-jointed chain (FJC):

$$\zeta_{\text{FJC}}(F) \equiv \frac{z}{L} = \coth\left(\frac{Fb}{k_{\text{B}}T}\right) - \frac{k_{\text{B}}T}{Fb} + \frac{F}{S}, \tag{2}$$

where b is the Kuhn length of the polymer. For a physiological salt concentration of $100\,\text{mM}$, the elastic parameters of ssDNA are given by $b = 1.55\,\text{nm}$, $S = 630\,\text{pN}$ (Bosco et al., 2013). In case of DNA, the contour length can be written as $L = Nl$, where N is the number of base(pair)s and l is the contour length per base(pair). Typical values are given by $l_{\text{ds}} \approx 0.34\,\text{nm}$ and $l_{\text{ss}} \approx 0.58\,\text{nm}$.

Since we are considering macrostates, the probability of each macrostate is calculated from the corresponding free energy G of that state, using the Boltzmann distribution. To

calculate the free energy G of each state we first need to calculate the free energy of the WLC and the FJC. These are given by

$$g_{\text{WLC}}(F) \equiv \frac{G}{L} = \int_0^F \zeta_{\text{WLC}}(F')\,dF' = F - \sqrt{\frac{Fk_{\text{B}}T}{A}} + \frac{F^2}{2S} \tag{3}$$

and

$$g_{\text{FJC}}(F) \equiv \frac{G}{L} = \int_0^F \zeta_{\text{FJC}}(F')\,dF' = \frac{k_{\text{B}}T}{b}\left(\log\left(\sinh\left(\frac{Fb}{k_{\text{B}}T}\right)\right) - \log\left(\frac{Fb}{k_{\text{B}}T}\right)\right) + \frac{F^2}{2S}. \tag{4}$$

The free energy of the ds-state is then given by the free energy of the DNA minus the decrease in potential energy caused by the bead that moves inside the magnetic field. This is given by

$$G_{\text{ds}}(F) = Nl_{\text{ds}}g_{\text{WLC}}(F) - F\Delta z = Nl_{\text{ds}}\left(g_{\text{WLC}}(F) - F\zeta_{\text{WLC}}(F)\right). \tag{5}$$

To calculate the free energy of the ss-state we need to consider which overstretching mechanism is used, peeling or melting. In case of peeling, the force F is directed through only 1 strand of ssDNA and in case of melting, the force F is directed through 2 parallel strands of ssDNA. The number of strands is then parametrized by $n_{\text{strands}} \in \{1, 2\}$, which equals 1 or 2 for peeling or melting. The free energy of the ss-state is then given by

$$\begin{aligned}
G_{\text{ss}}(F) &= n_{\text{strands}}Nl_{\text{ss}}g_{\text{FJC}}(F/n_{\text{strands}}) - n_{\text{strands}}(F/n_{\text{strands}})\Delta z + NG_{\text{bp}} \\
&= n_{\text{strands}}Nl_{\text{ss}}g_{\text{FJC}}(F/n_{\text{strands}}) - FNl_{\text{ss}}\zeta_{\text{FJC}}(F/n_{\text{strands}}) + NG_{\text{bp}} \\
&= N\left(n_{\text{strands}}l_{\text{ss}}g_{\text{FJC}}(F/n_{\text{strands}}) - Fl_{\text{ss}}\zeta_{\text{FJC}}(F/n_{\text{strands}}) + G_{\text{bp}}\right),
\end{aligned} \tag{6}$$

where G_{bp} denotes the average basepair disruption energy. As it turns out, the overstretching transition is not fully cooperative. A cooperativity factor c can be included by the following tranformation: $G \to cG$. By plugging the free energies in the Boltzmann distribution we can calculate the thermal average of the DNA extension by

$$\langle z(F) \rangle = \frac{Nl_{\text{ds}}\,\zeta_{\text{WLC}}(F)\,e^{-cG_{\text{ds}}(F)/k_{\text{B}}T} + Nl_{\text{ss}}\,\zeta_{\text{FJC}}(F)\,e^{-cG_{\text{ss}}(F)/k_{\text{B}}T}}{e^{-cG_{\text{ds}}(F)/k_{\text{B}}T} + e^{-cG_{\text{ss}}(F)/k_{\text{B}}T}} \tag{7}$$

where the number of basepairs N is the same for both states of course. When calculating the above in Python, it is vital a function like `scipy.special.softmax()` is used for numerical stability. This model can then be fitted to DNA overstretching data for both values of n_{strands} to see which one of the two fits best.

2.2 DNA unzipping: equilibrium statistical mechanics model

We can model the unzipping of DNA analogous to DNA overstretching, because it involves strand separation as well. In Figure 1 the geometry of a DNA unzipping template can be seen. From this figure it can be seen that the tensile force is directed through a piece of dsDNA anchored to a glass coverslip and the pieces of ssDNA resulting from the unzipping. The force does not go through the dsDNA hairpin.
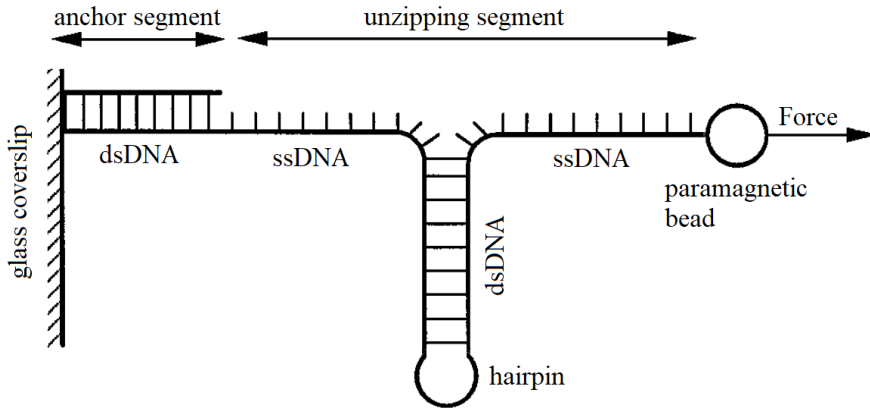
Figure 1: Geometry of DNA unzipping (adapted from Bockelmann et al. (1997)).

Using the geometry of Figure 1 and the fact that for every unzipped basepair the substrate gains 2 bases of ssDNA in length we can say that the extension of the DNA in unzipping configuration is given by

$$\langle z(F) \rangle = N_{\text{ds}} \, l_{\text{ds}} \, \zeta_{\text{WLC}}(F) + 2 \langle N_{\text{unzip}}(F) \rangle \, l_{\text{ss}} \, \zeta_{\text{FJC}}(F), \tag{8}$$

where N_{ds} is a constant and N_{unzip} is the number of unzipped basepairs. In thermodynamic equilibrium there would be a state for each unzipped basepair. But it turns out that unzipping is far from equilibrium and shows fully cooperative behaviour (see section 4.1), which means there are only two states: fully zipped and fully unzipped. Ignoring the kinetics, the energy difference ΔG between the two states is then given by

$$\Delta G(F) = N_{\text{unzip,max}} \left(2 l_{\text{ss}} g_{\text{FJC}}(F) + G_{\text{bp}} - 2 F l_{\text{ss}} \zeta_{\text{FJC}}(F) \right), \tag{9}$$

where $N_{\text{unzip,max}}$ is the maximum number of unzipped basepairs, i.e. the length in basepairs of the dsDNA unzipping hairpin. All contributions of the dsDNA part of the DNA substrate cancel out in the energy difference. Subsequently, we put the free energy in the Boltzmann distribution to get

$$\langle N_{\text{unzip}}(F) \rangle = \frac{0 \cdot e^{-0/k_{\text{B}}T} + N_{\text{unzip,max}} e^{-\Delta G(F)/k_{\text{B}}T}}{e^{-0/k_{\text{B}}T} + e^{-\Delta G(F)/k_{\text{B}}T}} = N_{\text{unzip,max}} \frac{e^{-\Delta G(F)/k_{\text{B}}T}}{1 + e^{-\Delta G(F)/k_{\text{B}}T}}$$
$$= N_{\text{unzip,max}} \left(1 + e^{\Delta G(F)/k_{\text{B}}T} \right)^{-1}. \tag{10}$$

The equilibrium model for DNA unzipping is then given by

$$\langle z(F) \rangle = N_{\text{ds}} \, l_{\text{ds}} \, \zeta_{\text{WLC}}(F) + 2 l_{\text{ss}} \, \zeta_{\text{FJC}}(F) N_{\text{unzip,max}} \left(1 + e^{\Delta G(F)/k_{\text{B}}T} \right)^{-1}. \tag{11}$$

This expression can easily be implemented in Python, no special functions are needed for numerical stability.

2.3 Localization of force barriers in DNA unzipping

In DNA unzipping, sequence-dependant force barriers can be visualized by determining the number of unzipped basepairs as a function of the force. Similar to what was done in Shundrovsky et al. (2006); Hall et al. (2009); Li and Wang (2012) for optical tweezers,

this can be done by mapping the measured extension and force to the number of unzipped basepairs. A reinterpretation of Equation (8) facilitates this. If z is the measured extension, we can solve for N_{unzip} to get

$$z(F) = N_{\text{ds}}\, l_{\text{ds}}\, \zeta_{\text{WLC}}(F) + 2N_{\text{unzip}}\, l_{\text{ss}}\, \zeta_{\text{FJC}}(F) \quad \rightarrow \quad N_{\text{unzip}} = \frac{z(F) - N_{\text{ds}}l_{\text{ds}}\, \zeta_{\text{WLC}}(F)}{2l_{\text{ss}}\, \zeta_{\text{FJC}}(F)}.$$
(12)

This mapping is allowed even when the unzipping and rezipping trajectories are not in equilibrium, as long the DNA is in mechanical equilibrium when fully zipped and fully unzipped. The next step in employing this technique is the localization of nucleosomes along the DNA sequence in chromatin.

2.4 Covalently binding DNA substrate to glass coverslip

Force spectroscopy experiments are typically limited by the lifetime of DNA tethers, which compromises reproducibility. Commonly used tethering methods result in a short lifetime due to the employment of non-covalent binding, which is weaker than covalent binding. For magnetic tweezers and atomic force microscopy, the DNA is often anchored to a glass surface making use of digoxygenin binding to anti-digoxigenin (Kaczmarczyk et al., 2020). Such a bond has a high chance of disruption for forces above 50 pN (Neuert et al., 2006). The bead attachment is often done however using a streptavidin-biotin bond, which is able to withstand at least 150 pN (de Odrowaz Piramowicz et al., 2006), not compromising the tethering lifetime. To create more robust tethers, techniques have been developed employing covalent bonding using thiol or amine functionalization of the DNA (Walsh et al., 2001). These techniques however require special buffers and suffer from nonspecific binding. Another approach making use of amine-functionalization does not suffer from nonspecific binding (Janissen et al., 2014). However this process is time consuming and requires many chemicals.

Gidi et al. (2018) proposed a simple and effective method of covalently attaching poly(ethylene glycol) (PEG) linkers to a glass surface using silane. Applying a silane-PEG coating to the glass requires minimal time and materials, and enhances surface passivation compared to conventional methods. In addition, Eeftens et al. (2015) demonstrated a novel way of covalently binding DNA, tagged with dibenzocyclooctyl (DBCO), to azide-functionalized PEG linkers. This approach comes with many advantages over the common tethering techniques mentioned above. The reaction is highly specific and bio-orthogonal, i.e. not interfering with biological processes, which makes this approach ideal for experiments *in vitro*. No catalyst is needed, which is often cytotoxic due to the presence of copper, and no special buffer is needed. Also, no non-specific binding occurs between the DNA and the anchoring structure. Here, we propose covalently tethering DNA to a glass microscope coverslip inspired by the work of Eeftens et al. (2015) and Gidi et al. (2018) to be used for magnetic tweezers. In our approach, a coverslip is coated with silane-PEG-azide tethers to which a DBCO-tagged DNA substrate can bind.
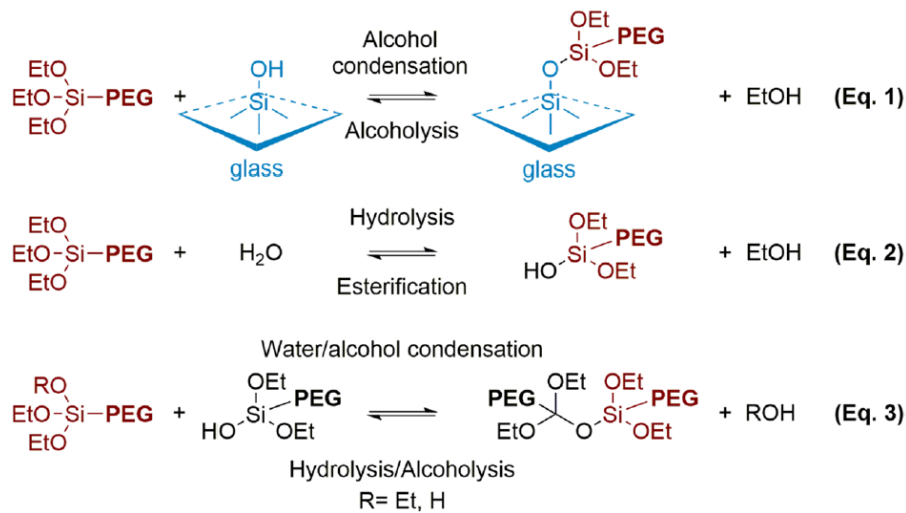
Figure 2: PEG-silane grafting reaction (1) and competing hydrolysis reactions with water (2) or newly generated PEG-silanol (3) (taken from Gidi et al. (2018)).

A problem that arises with this method is that silane hydrolyses in the presence of water (see Figure 2), resulting in the formation of hydrogen bonds rather than covalent bonds between the silane and the glass. This would form a weak spot in the setup, resulting in the disruption of the tether under high forces. To prevent this from happening, dimethyl sulfoxide (DMSO) is used as a solvent instead of water (Gidi et al., 2018). For this method to work, it is vital all traces of water are removed.

3 Materials & Methods

3.1 Covalently tethering DNA

3.1.1 DNA construct

One end of the DNA has to be labeled with biotin and the other end has to be labeled with DBCO (see section 2.4). For this reason, the pUC18 16×168 plasmid from which the DNA sample comes, was digested with BseYI and BsaI restriction enzymes. Afterwards, the DNA sample was purified using a promega clean-up kit. Next, a single DBCO molecule was incorporated at the BseYI restriction site using the Klenow reaction. Then, the sample was purified again using a promega clean-up kit and a single biotin molecule was incorporated at the BsaI site using the Klenow reaction. At last, the DNA sample was purified again using a promega clean-up kit. The 4753 bp DNA construct contains a sequence with a high affinity for the formation of nucleosomes. However, this DNA construct was only used for naked DNA experiments.

3.1.2 DNA immobilization

One point of a DNA substrate is tagged with biotin, which binds strongly to a streptavidin-coated paramagnetic bead. Another point of the DNA is tagged with DBCO. A glass microscope coverslip is coated with silane-PEG-azide (SPA). The silane end of the SPA covalently binds to the glass. In turn, the azide end of the SPA covalently binds to the DBCO, creating covalently tethered DNA that can be studied using magnetic tweezers. The tethering structure is shown in Figure 3.
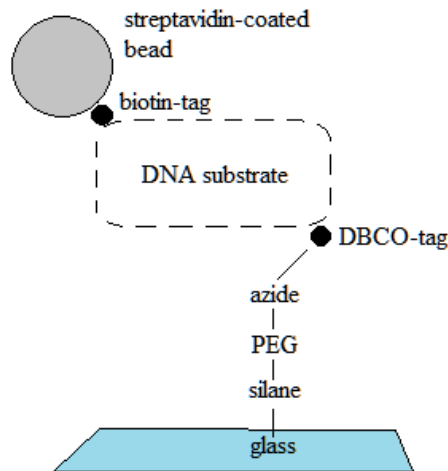
Figure 3: Covalently tethering DNA substrate to glass microscope coverslip, inspired by Eeftens et al. (2015) and Gidi et al. (2018).

3.1.3 Sample preparation

First, the coverslips (bottom coverslip: $24 \times 60 \, \text{mm}^2$, thickness #2; top coverslip: $24 \times 40 \, \text{mm}^2$, thickness #1.5) were cleaned with a UVO cleaner (Jelight Company, USA, model No. 42A-220) for 10 minutes. The cleaned coverslips were put into a Petri dish afterwards, containing a dessicant (calcium chloride) and pre-heated at 90 °C for 10 minutes. In the meantime, a 0.1 mol% SPA (silane-PEG-azide) in DMSO solution was prepared. When the coverslips were done pre-heating, $\sim$ 0.5-1 mL of the 0.1 mol% SPA in DMSO

solution was pipetted on the coverslips, covering all surfaces. The heating was continued at 90 °C for 30 minutes. In the meantime, a solution containing the DNA substrate and the paramagnetic beads was prepared. The solution consisted of 1 µL of bead solution (streptavidin-coated, paramagnetic M-270 DynaBeads; Invitrogen, USA); a DBCO- and biotin-tagged DNA substrate solution (the amount was optimized depending on the experiment); and 200 µL of measurement buffer (ESB). The buffer consisted of: 10 mM HEPES, 100 mM KCl, 0.1% (= 1 mg mL^{-1}) Tween20, 0.2% (= 2 mg mL^{-1}) BSA. The incubation happened at room temperature inside a rotator for 15 minutes. This was done to prevent the beads from sinking to the bottom. When the coverslips had been heated for 30 minutes, they were rinsed with $\sim$ 1 mL HPLC water to remove excessive SPA, and dried using an N$_2$ flow/spray gun. Next, the flowcells were assembled. In each flowcell channel, 50 µL of the DNA substrate and beads solution was flushed. The incubation happened at room temperature for 30 minutes, facilitating the DBCO-azide click chemistry reaction.

3.2 Conventional tethering for DNA unzipping

3.2.1 DNA construct and immobilisation

A DNA unzipping construct was made that consists of a 685 bp anchoring segment and a 2969 bp unzipping hairpin (see Figure 1). A conventional tethering approach was taken for the DNA unzipping experiments, making use of a single DIG:Anti-DIG bond (see section 2.4). Therefore, the anchoring segment is labeled with DIG. The DIG binds to an Anti-DIG-coated coverslip. An LNA probe connected to the other end of the unzipping hairpin was used to attach the DNA to the bead. This LNA probe contains a small closed hairpin at its end with biotin on top of the hairpin. The biotin binds to a streptavidin-coated paramagnetic bead. The details of this construct are explained elsewhere (Heinsman, 2017).

3.2.2 Sample preparation

First, the flowcell was assembled with stickers (no coverslips yet). Next, the coverslips (same a described in subsection 3.1.3) were cleaned using Milli-Q water using a coverslip jar, followed by ethanol using another jar. The coverslips were then assembled on the flowcell. A $10\,\mu g\,mL^{-1}$ Anti-DIG solution in PBS was prepared. For each flowcell channel, $60\,\mu L$ of the Anti-DIG solution was flushed in. Only $50\,\mu L$ fits inside the channel. The extra bit was used to fill the in- and output tubes of the channel with liquid to prevent the formation of bubbles inside the channel. From here on in the protocol: pipetting into the channels of the flowcell was done very slowly. Too high currents in the flowcell channel, causing too high forces on the tethers would disrupt them. The flowcell was then incubated for 2 hours at $4\,°C$. The incubation time could be increased for better results. Afterwards, the channels were rinsed with $200\,\mu L$ of 4% BSA. This was incubated for 2 hours at $4\,°C$ as well. A DNA-substrate solution was prepared as described in subsection 3.1.3, but the beads were left out. When the incubation time was over, each channel was rinsed with $200\,\mu L$ of ESB measurement buffer. $60\,\mu L$ of the DNA-substrate solution was flushed in each channel that was needed for the experiment.

3.3 Magnetic tweezers

3.3.1 Experimental setup

The magnetic tweezers that were used (see Figure 4), consist of two magnets that can be moved together in the z-direction. A collimated light beam from an LED shines down between the magnets, through the top coverslip of the flowcell, onto the DNA sample. The flowcell is screwed on a mounting stage by which the flowcell can be translated in x, y-directions. The light leaves the flowcell through the bottom coverslip and enters the microscope objective, for which a drop of immersion oil is needed, suspended between the flowcell and the objective. The light then shines via a mirror onto a CMOS sensor. Further details of the setup can be found in Brouwer et al. (2018); Kaczmarczyk (2019).
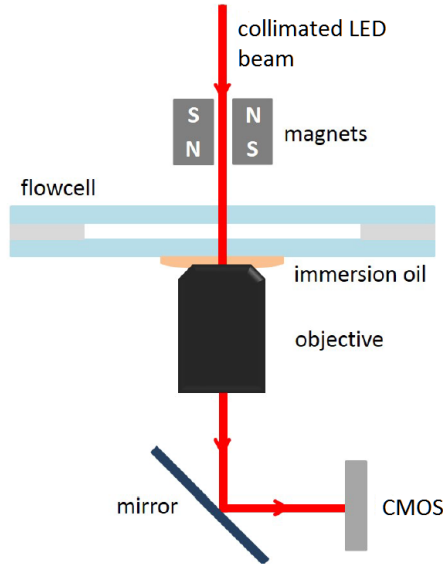
Figure 4: Schematic of magnetic tweezers setup, adapted from Vendel (2015).

A custom flowcell was used for the experiments. The frame of the flowcell is made of white Perspex. A white sticker with three carved-out channels covers the bottom of the frame. A layer of double-sided adhesive foil with carved-out channels then covers the white sticker. The bottom of the flowcell is sealed off by a $24 \times 60\,\mathrm{mm}^2$ glass microscope coverslip of thickness #2. The flowcell frame contains a $24 \times 40\,\mathrm{mm}^2$ hole. On the topside of the flowcell a $24 \times 40\,\mathrm{mm}^2$ coverslip of thickness no. 1.5 fits into the hole and sticks to the sticky side of the white sticker. In this way, three transparent channels of $\sim 50\,\mathrm{\mu L}$ are formed that can be accessed by in- and output tubes, carved out in the frame.

3.3.2 Force calibration and calculation

The magnetic force on the paramagnetic bead is a nonlinear function of the distance between the bead and the magnet, which is difficult to calculate analytically. For this reason and the fact that the force on the bead needs to be calibrated, this relation is found experimentally. If for different magnet heights the z-position of the bead and the mean-square deviations in the x- or y-direction are measured, the force on the bead as a function of the height h can be determined. Further details are found in Brouwer et al. (2018). The relation between force and extension is then given by a double exponential (Yu et al., 2014) and is uniquely determined by the type of magnets and paramagnetic

beads used. This relation was determined to be

$$F = F_{\max} \left(0.7 \exp\left(-\frac{h}{L_1}\right) + 0.3 \exp\left(-\frac{h}{L_2}\right) \right) + F_0,$$

$$F_0 = 0.01\,\mathrm{pN}, \quad L_1 = 1.4\,\mathrm{mm}, \quad L_2 = 0.8\,\mathrm{mm}, \tag{13}$$

$$F_{\max} = \begin{cases} 9\,\mathrm{pN} & \text{if } 1.0\,\mathrm{\mu m} \text{ beads are used,} \\ 85\,\mathrm{pN} & \text{if } 2.8\,\mathrm{\mu m} \text{ beads are used.} \end{cases}$$

In this work, only 2.8 μm beads were used. Using this relation, force-extension plots can be made of magnetic tweezers data of DNA.

3.4 Data collection and analysis

Before each measurement with the MT, all beads in the field of view (FOV) ($543 \times 544 \, \mu m^2$) can be automatically detected, by their characteristic diffraction pattern. During the measurement, each bead is tracked by a special FFT-phasor algorithm by which each bead is traced in 3D with nanometer precision (Brouwer et al., 2020). The time and magnet height are recorded as well.

Because of the difficulty of implementation in Python and the high risk of false outcomes, the categorization was done manually. Each bead was categorised as "stuck", "loose" or "extendable", by looking at its extension versus time curve. Archetypal examples of these categories are shown in Figure 5. Stuck is when z does not rise more than $\sim 30\%$ of the contour length above the baseline over time, and a bead is visible before and after the measurement. Loose is when before the measurement a bead is visible, and after the measurement the bead is gone. From the moment of rupture on, the extension-time curve will show a large variance in z of order $\sim 10 \, \mu m$. This indicates that the software returns random z-positions after disruption of the tether, since it cannot detect a bead. Extendable is when z rises more than $\sim 50\%$ of the contour length above the baseline, and only one bead is visible before and after the measurement. Preferably, z follows a WLC in a force-extension curve. This is not a requirement however, since we focus on tethering quality. Some of the extendable tethers are categorised as "overstretching". The force-extension curve of those tethers shows a plateau at $\sim 65 \, pN$. This can only happen for a single tether since the maximum force of the MT is $85 \, pN$. If the force would be divided over two or more tethers, the force needed for overstretching cannot be reached, which means that such a force plateau indicates a single DNA tether.

In the beginning of the research it was noticed that when looking at the force plateau in force-extension curves of overstretching tethers, the backward curve lied above the forward curve. This is physically impossible. This can happen if the recorded magnet position is not fully synchronized with the actual magnet position. This issue can be solved by time shifting the magnet height array a few steps. The amount of shifting was manually adjusted to obtain the best overlap between the full forward and backward curves.

Using least-squares fitting, a model function was fitted to the force-extension data. For optimal fitting performance, an initial guess needs to be given for each fit parameter. The result of a previous fit or a manual fit, or values from literature can be used for this.
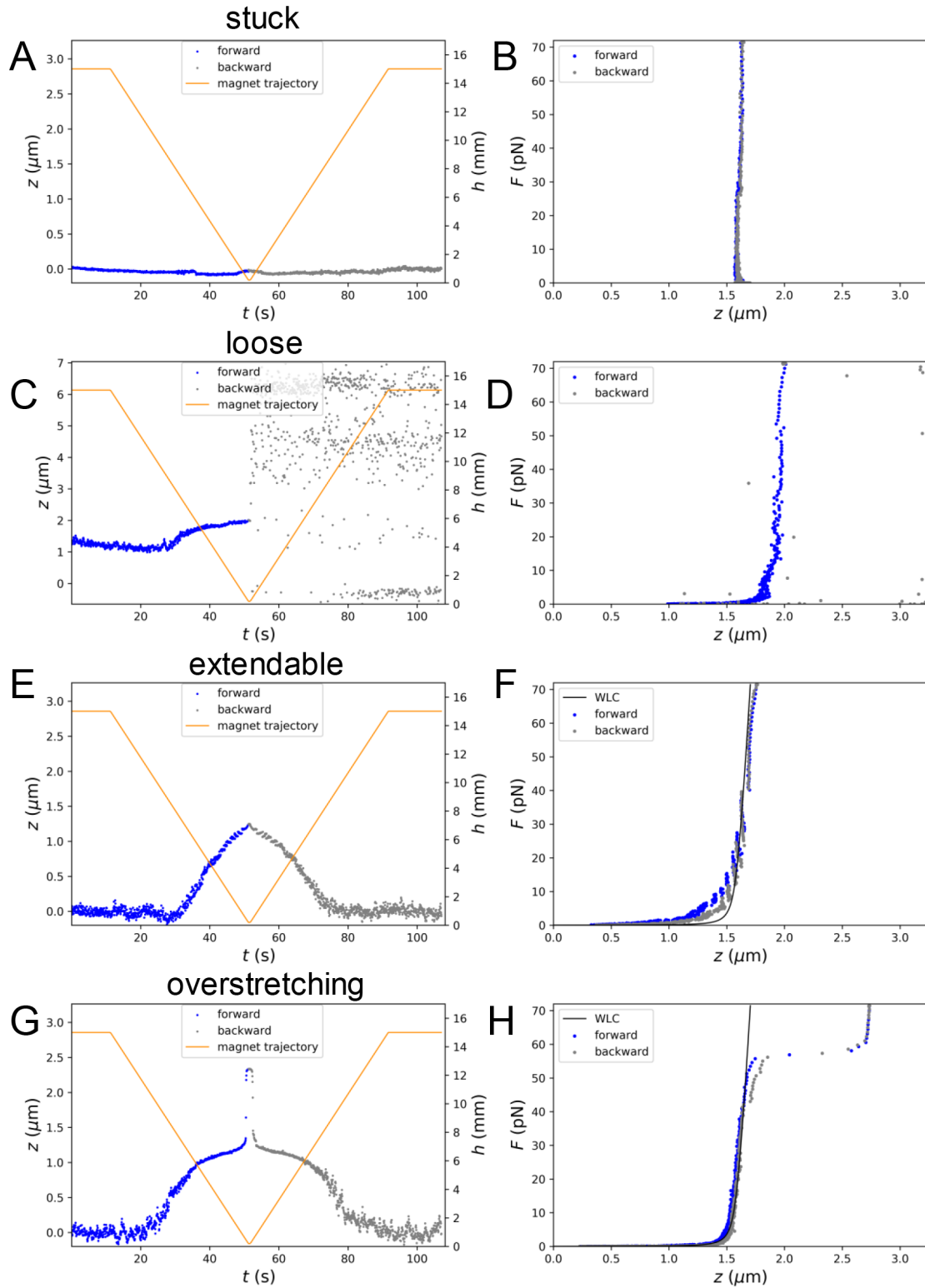
Figure 5: **Archetypal examples of bead categorization:**
A DNA sample with a contour length of $1.6\,\mu m$ ($4753\,bp$) was used to do these measurements. The contour length gives an estimate of the expected scale of the extension to be measured. A) Extension-time curve of stuck bead. B) Force-extension curve of stuck bead C) Extension-time curve of loose bead. This curve is not drift corrected. D) Force-extension curve of loose bead. This curve is not drift corrected. E) Extension-time curve of extendable bead. F) Force-extension curve of extendable bead. A WLC was fitted to the data. G) Extension-time curve of overstretching bead. H) Force-extension curve of overstretching bead. The overstretching plateau can clearly be seen. A WLC was fitted to the data.

4 Results

4.1 Covalently binding DNA substrate to glass coverslip results in low experimental yield

In DNA force spectroscopy, the short lifetime of common tethering techniques is sometimes limiting the experiment. A new protocol aims to solve this issue by the employment of silane-poly(ethylene glycol) (PEG)-azide (SPA) to covalently tether DNA to the surface and to ensure surface passivation (see section 3.1.3). Since silane hydrolyses in the presence of water, resulting in the formation of hydrogen bridges instead of covalent bonds, dimethyl sulfoxide (DMSO) was used as a solvent. Using magnetic tweezers (see section 3.3) we explored the use of this novel approach to facilitate force spectroscopy on DNA substrates.

Since traces of water in the sample should impede the formation of covalent tethers, we compared two batches of DMSO containing different trace amounts of water. This comparison is shown in Figure 6A. We are only concerned with DNA tethering to one bead, in which case the tether will overstretch (see section 2.1). Figure 6A shows that the anhydrous DMSO yields a few more overstretching and extendable tethers (see section 3.4) than DMSO with an unknown amount of H_2O. This could indicate that anhydrous DMSO indeed contains less water than DMSO that was not purchased as anhydrous, resulting in more single tethers. For this reason we continued the experiments using anhydrous DMSO. In the beginning of the research, almost no extendable tethers were observed, only stuck and loose beads. Water may have accumulated in reused SPA dilutions, so we made fresh SPA dilutions for each experiment. Using such fresh solution, extendable tethers were visible. Also, to get extendable tethers, all stock materials were vortexed at ~ 1000 rpm for about two seconds, except for the ESB buffer, since it is prone to bubble forming. This suggests that the presence of water impedes proper surface functionalization, what can be overcome by using anhydrous DMSO and fresh SPA dilutions.

Too much DNA can result in multiple DNA tethers being attached to the same bead. For this reason, we also compared the experimental yield of two different DNA concentrations, which is shown in Figure 6A. $400\,\mathrm{pg\,\mu L^{-1}}$ DNA yields a similar amount of tethers as $50\,\mathrm{pg\,\mu L^{-1}}$. Thus, an $8\times$ increase in DNA concentration does not change the yield. To prevent wasting material we continued experiments using a DNA concentration of $50\,\mathrm{pg\,\mu L^{-1}}$.

In Figure 6A, the variation in experimental yield between two measurement days was considerable. Therefore we investigated the variability of the experimental yield over a period of weeks. Figure 6B shows that the day-to-day variation in the number of overstretching and extendable tethers was larger than the error bars of each experiment. However, experimental parameters were sometimes adjusted. On 16 January the SPA stock was not vortexed for example. Nevertheless, the large variation over time suggests there are unknown factors influencing the yield of DNA tethering.

Due to the variation in yield we investigated the quality of the SPA coating. The reactive -OH groups at the surface of the glass coverslip can be obstructed by impurities. These potential impurities can be removed by etching the glass before applying a SPA coating. To verify this, experiments were done where the coverslip was etched and coated, etched only, and not treated at all. As a control experiment, we also did the experiment without DNA (beads only). These results are shown in Figure 6C. Remarkably, extension was

observed when no DNA was added. This can happen however since stuck beads can still show extension of a few hundred nanometers. This could result from a balance between the magnetic force and adhesive forces from the surface. Also, loose beads were not flushed out before measurement to prevent applying an uncontrollable amount of stress on the SPA tethers during the flushing. These loose beads accumulated and sometimes showed extension upon applying a force, which could be a result of dipole-dipole interactions balanced by the magnetic force gradient. Such accumulations were normally excluded from analysis based on their deviating diffraction pattern. The number of extendable tethers seemed to slightly increase when more treatments had been done to the glass. When comparing the number of extendable tethers with DNA, to those with beads only, the yield of no-treatment and etching-only looks the same. When etching and coating is done, the DNA experiments have a slightly higher yield than the beads-only experiments. This means that most of the extendable DNA tethers are aspecifically bound to the surface.

In order to investigate the quality of the surface passivation with SPA, the number of stuck beads for each of the above mentioned experiments is added to Figure 6C. One expects the number of stuck beads to go down when the glass is treated with SPA, due to surface passivation. However, the number of stuck beads is always higher when the SPA treatment was done compared to no treatment. When the glass was only etched, the amount of stuck beads varied wildly. The number of stuck beads seemed to behave randomly with respect to the treatment of the coverslip, which is unexpected.

The protocol should result in the formation of tethers that are covalently bound to the surface, resulting in a decrease in the number of tethers that break loose when a force is applied. Figure 6C shows that the amount of loose beads however stayed larger no matter what treatment was applied to it. Most of these loose beads had a typical DNA force extension curve before they broke. Therefore, it is likely these tethers were either not covalently bound to the SPA or the SPA was not covalently bound to the glass.

The expected trends were not observed. For example, more treatments did not reduce the number of stuck beads and the number of extendable tethers did not go up. Instead the number of extendable tethers remained low and the number of stuck beads and loose tethers behaved randomly. Thus, there are still unknown factors influencing the yield of the experiment. Nevertheless, we could find typically 10 well-behaved tethers per field of view, and we proceeded with these to learn more about DNA melting.
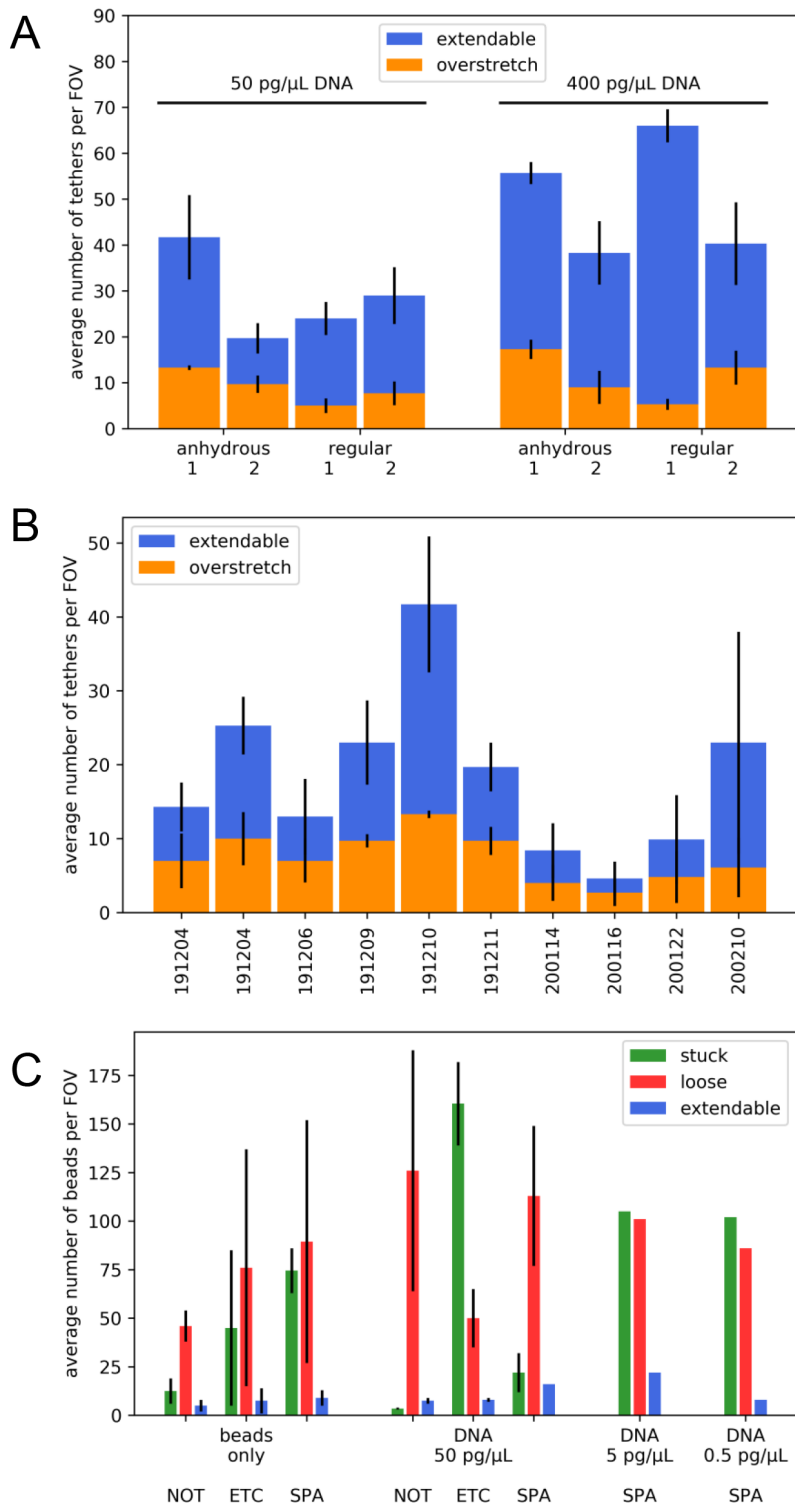
Figure 6: **Covalent DNA tethering results in low experimental yield due to unknown factors:**
A) Flowcell quality is shown in terms of the number of extendable tethers (blue), averaged over multiple FOVs for different DNA concentrations and batches of DMSO (anhydrous and regular), on two different days. The extendable tethers that show overstretching behaviour in a force-extension curve are depicted in orange. The bars are not stacked, since overstretching tethers are also extendable. B) Flowcell quality over time, for $50\,\mathrm{pg}\,\mu\mathrm{L}^{-1}$ DNA and anhydrous DMSO. C) Comparison of the flowcell quality for three different treatments of the glass coverslip: no treatment (NOT), etched only (ETC), and etched and SPA-coated (SPA). It is also indicated how many beads stick to the surface (stuck), how many beads/tethers detach from the surface (loose) during the measurement, and how many tethers are extendable. This is done for beads only and for $50\,\mathrm{pg}\,\mu\mathrm{L}^{-1}$ DNA. For beads only, extendable means beads showing extension. The error bars result from averaging over two different flowcells made on the same day. No error bars indicate that only one flowcell was measured.

4.2 Two-state model for dsDNA overstretching

When DNA overstretches, basepairs are split by two different mechanisms that we call "peeling" and "melting" (see section 2.1), which are visually represented in Figure 7B. These pathways lead to two conformations which we included in a new two-state statistical mechanics model. The model can be fitted to force extension curves of DNA overstretching experiments, performed using magnetic tweezers. We used the contour length per base of ssDNA l_{ss} and the average basepair disruption energy G_{bp} as fitting parameters. These values define the shape of the force-extension curve of overstretching DNA but are poorly documented as compared to other parameters.

A plot of a typical force-extension curve of an overstretching dsDNA tether is shown in Figure 7A. The two states, normal B-DNA and overstretched DNA, are clearly visible as the part of the data that follows the WLC curve and the part of the data that follows the two FJC curves, denoting each of the two DNA conformations. The overstretching plateau is clearly visible between $50\,\mathrm{pN}$ and $60\,\mathrm{pN}$. When looking at Figure 7A one can immediately see why it is so difficult to distinguish the peeling from the melting model when looking at the force-extension curve. The data follow the WLC-curve nicely before overstretching. After overstretching it should follow one of the two FJC-curves, but above $\sim 50\,\mathrm{pN}$ the two curves lie on top of each other.

A fit to the force-extension curve of a single measurement results in a value for each fit parameter and the corresponding standard error of the fit. Approximately 300 different single dsDNA tethers that show overstretching were measured. Histograms of the values found for the fit parameters for both models are shown in Figure 7C and D. The standard deviations of these histograms were calculated as well. For each of the fitted parameters, the mean and the standard error of the fit were calculated. The results are given in Table 1.

model	parameter	mean	SE of fit	SD of histogram
peeling	l_{ss} (nm)	0.538	0.003	0.02
	G_{bp} ($k_B T$)	1.162	0.009	0.07
melting	l_{ss} (nm)	0.588	0.004	0.02
	G_{bp} ($k_B T$)	1.645	0.012	0.09

Table 1: **DNA overstretching fit parameters:**
These parameters were obtained by fitting ~ 300 force-extension curves of dsDNA tethers to the two-state model (Equation (7)).

It is interesting that the standard deviations of the histograms are about six times larger than the means of the standard errors of the fits, i.e. the spread in the data is larger than the error in the fit. This could mean that there are unknown sources of variation in the experiment.

Figure 7A shows that the overstretching transition is not fully cooperative, i.e. the transition happens gradually. Physically, this can only happen when several melting bubbles arise and coexist, at different places along the sequence. This is parameterized by a cooperativity factor c (see Equation (7)). It was manually adjusted to $c = 0.07$ to obtain the best visual match at the transition near the overstretching part of the curve. This parameter has no impact on the value of G_{bp} or l_{ss}. Thus, the two-state model seems

to accurately describe DNA overstretching, and despite its simplicity it recovers plausible values for the contour length of ssDNA and the basepair melting energy.
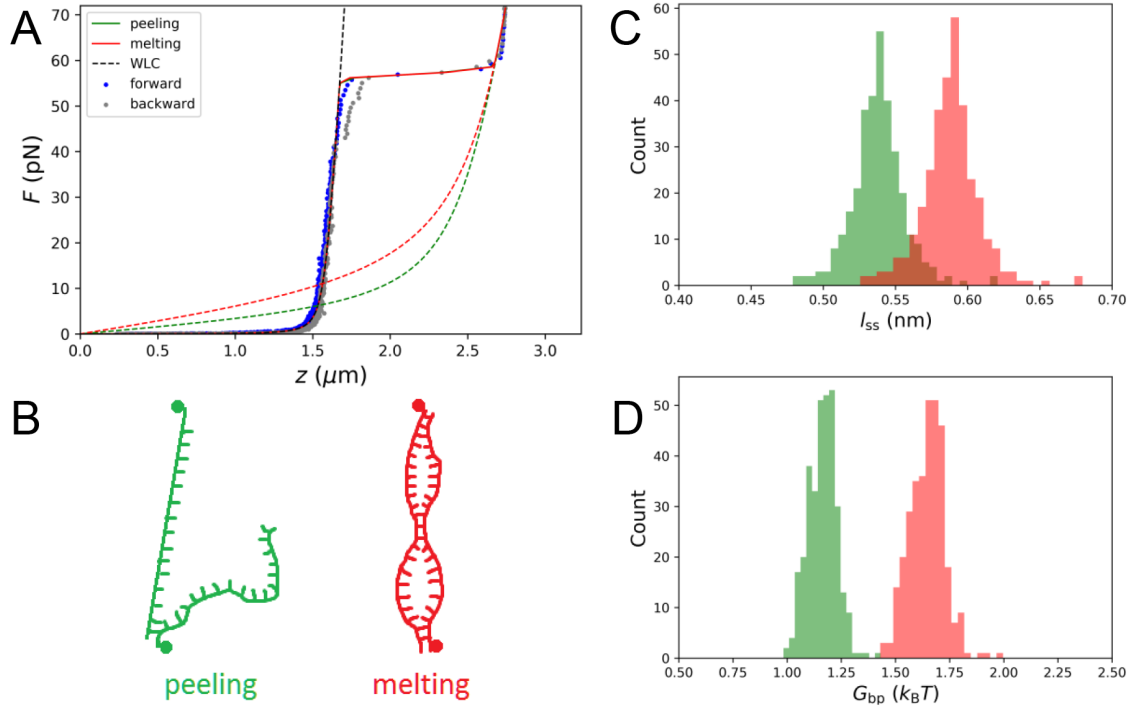
Figure 7: **Peeling and melting models of mechanical structure of overstretching DNA completely overlap when fitted to data:**
A) This is a typical force-extension curve of overstretching dsDNA. The blue dots (forward) denote the data points during stretching and the grey dots (backward) denote the relaxation. Two states can be observed: the normal B-DNA like state that follows a WLC (WLC dotted in black) and the overstretched state that behaves like ssDNA following either of two FJCs (FJCs dotted in green and red). Two different models have been fitted to the data: a "peeling" of the strands and a partial "melting" of the strands model. The solid curves of these models completely overlap. B) The DNA conformations of peeling and (partial) melting of the strands after overstretching is shown. C/D) Histograms of the fitted values of l_{ss} and G_{bp} (see section 2.1) are shown for both models.

4.3 Localizing force barriers during DNA unzipping

The DNA substrate used for the unzipping experiments consisted of a 685 bp dsDNA anchoring segment and a 2969 bp dsDNA unzipping hairpin (see Figure 1). Before unzipping an extension of $\sim 200\,\text{nm}$ is expected and after unzipping an extension of $\sim 3.5\,\mu\text{m}$ is expected. Figure 8A shows a force-extension curve of the dsDNA unzipping experiment. At $15\,\text{pN}$ the DNA starts to unzip. The unzipping curve (forward) lies above the rezipping curve (backward), which indicates hysteresis. Thus, the sample was not in thermodynamic equilibrium during unzipping and rezipping. When fully zipped or fully unzipped, the forward and backward curves do lie on top of each other, which means during these epochs the DNA was in mechanical equilibrium.

We fitted a combination of a WLC-FJC to the fully unzipped part of the data (see Equation (8)). The contour length per base l_{ss} of ssDNA was set to $0.59\,\text{nm}$ (see Table 1). The Kuhn length of ssDNA b_{ss} and an offset z_0 were used as fit parameters. The offset is needed because the tether can be attached at any place on the "southern hemisphere" of the bead. A histogram of b_{ss} is given in Figure 8B and it is summarized in Table 2. Using the fitted offset, a WLC for the zipped hairpin can be plotted. The model does not align with the data in the low force regime. This may be due to excluded volume and other surface interactions that were not included.

In the unzipping curve a force plateau is observed at $15\,\text{pN}$. In this plateau the DNA transitions from a duplex to a melted conformation, similar to DNA overstretching. However, the unzipping is not in equilibrium, so an equilibrium model may not be used to describe the curve. Ignoring this theoretical remark, the equilibrium model from Equation (11) was fitted to the forward and backward data, and the average basepair disruption energy G_{bp} was computed. This yields upper and lower bounds for the equilibrium value of G_{bp}. The fits are plotted in Figure 8A as well. A histogram of the fitting results is given in Figure 8D and they are summarized in Table 2.

parameter	mean	SE of fit	SD of histogram
b_{ss} (nm)	1.49	6.6×10^{-2}	0.21
G_{bp} (forward) ($k_B T$)	1.05	1.7×10^{-6}	0.10
G_{bp} (backward) ($k_B T$)	0.86	1.2×10^{-6}	0.08

Table 2: **DNA unzipping fit parameters:**
These parameters were obtained by fitting ~ 100 force-extension curves of dsDNA tethers to equilibrium models (Equations (8) and (11)).

We next mapped the extension z to the number of unzipped basepairs N_{unzip} using Equation (12). The result is shown in Figure 8C. In the figure, at $N_{unzip} \approx 0$ and $3000\,\text{bp}$, almost vertical lines can be seen, indicating a constant number of unzipped basepairs before and after unzipping. It does not matter if the unzipping happens in equilibrium or not for this mapping to work, as long as the fully unzipped part of the data can be fitted to Equation (8). The data below $5\,\text{pN}$ was ignored because the data are affected by bead surface interaction at this range of force.

In Figure 8A and C clusters of data points can be seen during the unzipping and rezipping trajectories. To obtain better statistics a histogram of N_{unzip} was made from ~ 100 curves, shown in Figure 8E. The peaks in the histogram depict barriers for un/rezipping. The large peaks at $N_{unzip} \approx 0$ and $3000\,\text{bp}$ correspond to the fully zipped and unzipped

states. The clustering of data points results from maxima and minima in the free energy landscape of the DNA substrate, caused by the local accumulation of GC basepairs, since a GC bond is stronger than an AT bond. The local GC fraction of the sequence was calculated and shown in Figure 8E as well. Histogram peaks of the backward data seem to match troughs in the local GC fraction. Only small histogram peaks appeared in the forward data. Overall, mapping the extension to the number of unzipped basepairs was effective in localizing force barriers along the sequence.
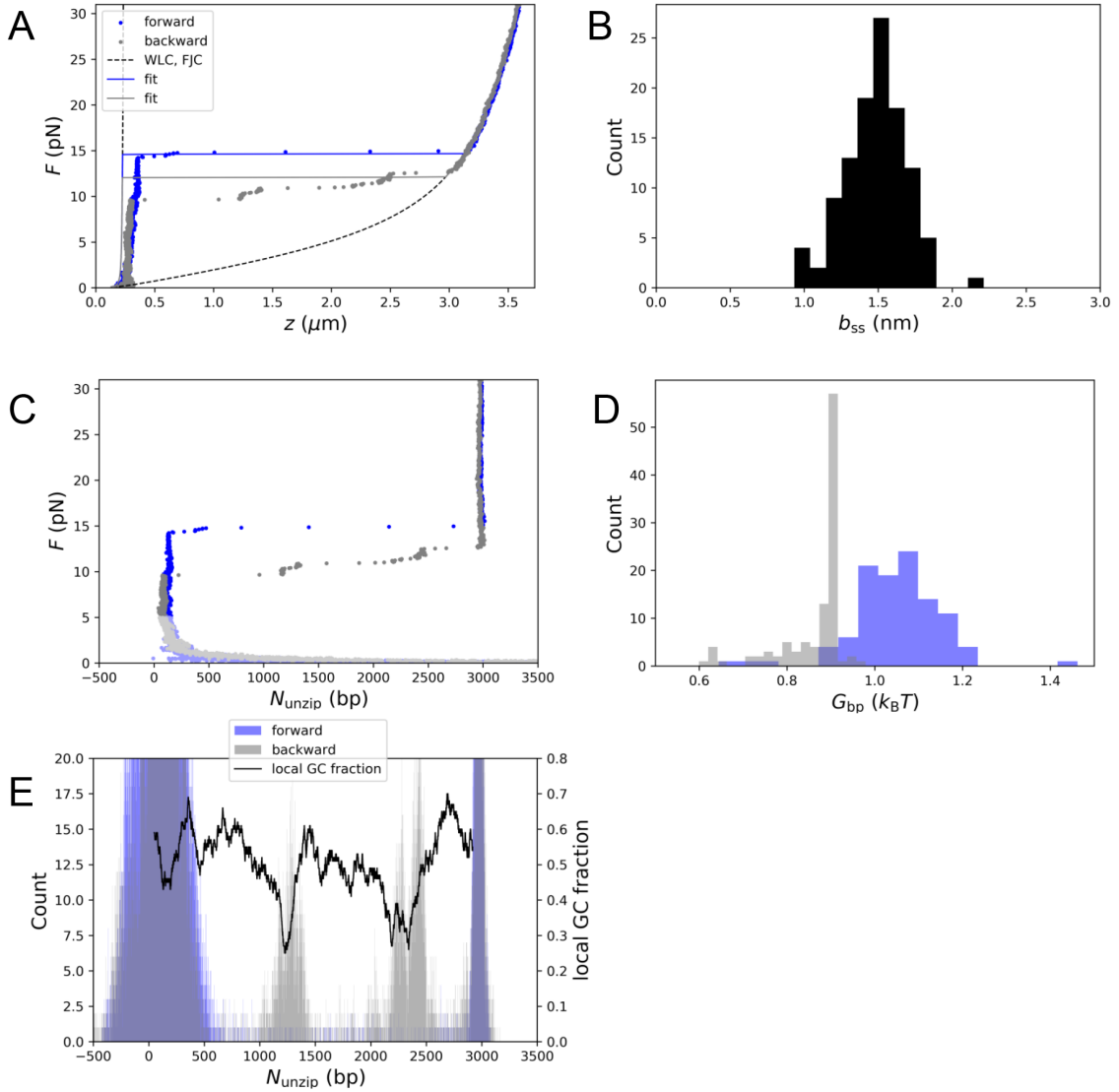
Figure 8: **Localized force barriers in DNA unzipping match local GC fraction in sequence:**
A) This is a force-extension curve of dsDNA being unzipped, due to the presence of a hairpin. Only two macrostates are observed in the transition between fully zipped and fully unzipped. However, clustering of data points during the transition is observed. When fully unzipped, a WLC + FJC nicely fits the data. From this, the Kuhn length bss of ssDNA was obtained. Although the transition is not in equilibrium (hysteresis) an equilibrium model was fitted to the full forward and backward curves to get upper and lower bounds for G_{bp}. B) A histogram of the fitted values of b_{ss} is shown for measurements of individual molecules. C) Using Equation (12), the extension z was mapped to the number of unzipped basepairs N_{unzip}. A vertical rise indicates a stationary number of unzipped basepairs. Below ~ 5 pN, the model does not describe the data correctly (depicted in a lighter hue). D) A histogram of the fitted values of G_{bp} is shown for the forward and backward data. E) For all measurements of individual DNA molecules a histogram was made for the number of unzipped basepairs. A cutoff below 5 pN was used to exclude the incorrectly mapped data. Peaks in the forward and backward data denote local maxima and minima in the free energy. The local GC fraction of the hairpin is shown as well, which is calculated with a moving window of width 100 bp.

5   Discussion & Conclusion

The investigation that was done on sample preparation yielded a large variation in tethering quality. No expected trend could be observed in the passivation quality either. The protocol appeared to be unreliable. The two-state DNA overstretching model was successful in describing the data. The different overstretching mechanisms seemed difficult to distinguish. The equilibrium unzipping model yielded reasonable upper and lower bounds of the fit parameters. Force barriers were localized during unzipping, by use of a special mapping of the data.

5.1   Covalently binding DNA substrate to glass coverslip results in low experimental yield

In a DNA unzipping experiment (see section 4.3) with different DNA, where the Anti-DIG protocol (see section 3.2) was used, we observed 81 extendable tethers per FOV of which 36 where single tethers (data not shown), which is much higher than 18 extendable and 7 single tethers on average as shown in Figure 6B. Gidi et al. (2018) (the work on which the protocol was based) measured ~ 35 fluorescently tagged silane-PEG tethers of which 81% were single tethers in an area of $2500\,\mu m^2$, which is 118 times smaller than our FOV. In our FOV that would equate to ~ 4100 extendable tethers of which ~ 3300 are single tethers. Thus, the tethering quality we obtained is much lower than what was obtained in literature. This asks for a more extensive investigation of the quality of the surface functionalization and passivation. This could be done by fluorescence microscopy experiments, in which the SPA tethers can be labeled as fluorophores.

The protocol we used differs slightly from Gidi et al. (2018). They first cleaned the coverslips using a piranha solution for 90 minutes. Then they etched with NaOH for 30 minutes. After that they soaked the coverslips in dry acetone. They claim this was crucial in counteracting the hygroscopic nature of the glass. They also had better results during their extremely dry winter. We did not do piranha cleaning. We did soak the coverslips in acetone after etching. This could mean that the exposure of the coverslips to air before the SPA is applied, has to be minimalized. We pre-heated the coverslips in the oven for 10 minutes before applying the SPA coating. In this step water from the air could still have accumulated on the coverslips. Also, when the SPA-coated coverslips had been in the oven for 30 minutes, we rinsed the coverslips with HPLC water. According to Gidi et al. (2018), the silane-PEG grafting reaction (see Figure 2) is reversible. This could mean that when water was directly applied to the surface of the coverslips after the coating had been applied, some of the coating came off.

The yield that was obtained in covalent tethering experiments of DNA leaves something to wish for. Nevertheless, on average we did find about 10 tethers per FOV that survived forces of $71\,pN$ that could be used for studying DNA overstretching. By investigating the surface treatment, this amount could be increased in the future, facilitating long-lifetime samples.

5.2   Two-state model for dsDNA overstretching

Only the data above $50\,pN$ can show which overstretching mechanism is favored, since below $50\,pN$ the data follows a WLC for both mechanisms. The melting model yields $l_{ss} = (0.59 \pm 0.02)\,nm$, which is similar to a 1.7 times increase (no error given) in contour length when overstretched as given in literature (Smith et al., 1996; Cluzel et al., 1996; Marko and Neukirch, 2013). Also the value found for $G_{bp} = (1.65 \pm 0.09)\,k_BT$ agrees with

$1.69\,k_{\mathrm{B}}T$ (no error given), which was calculated from enthalpy and entropy changes of terminal GC and AT basepairs given in SantaLucia (1998), for melting. The value of G_{bp} is however strongly buffer dependant (Smith et al., 1996). However, during overstretching, the DNA could also partly consist of melting bubbles and partly of unpeeled DNA, or the DNA could be in the S-DNA form (King et al., 2013), although this is not favored for the salt concentration we used. The model does not capture this behaviour. For this reason, the model is not able to distinguish the actual microscopic nature of the DNA that was measured. The heuristically introduced cooperativity factor deserves a derivation using statistical mechanics. The number of melting bubbles that coexist could be included as a statistical parameter. A nearest-neighbour interaction could be used to model the basepair disruption. The cooperativity factor could also be omitted due to its small effect.

The two-state DNA overstretching model is similar in design to the chromatin folding model by Meng et al. (2015), which successfully models force-extension data of chromatin stretching (Kaczmarczyk et al., 2020). The two-state model successfully describes the overstretching transition of DNA.

5.3   Localizing force barriers along DNA during unzipping

When looking at the histogram of the found values for G_{bp}, one notices that the values corresponding to the backward data are sharply peaked around its mean. This is probably due to the fact that the rezipping trajectory does not follow a straight line in the force-extension curve, like the equilibrium model. In such a case, the least-squares fitting algorithm is prone to linger at local minima. Comparing the results of fitting the equilibrium model, to the values obtained with DNA overstretching, shows that G_{bp} is a bit higher for overstretching but it has the same order of magnitude.

The value of b_{ss} is buffer dependent. The found value, $b_{\mathrm{ss}} = (1.49 \pm 0.21)\,\mathrm{nm}$ is in agreement with Bosco et al. (2013) for a salt concentration of $100\,\mathrm{mM}$. The local GC fraction of the sequence was calculated similarly to Heinsman (2017). The DNA sample used in all unzipping experiments was the same as used by Heinsman (2017) and the results of the backward data are also similar, the results of the forward data are not. This means that only minima and not maxima of the free energy landscape are observed. This is probably due to the fact that the unzipping did not happen in equilibrium as a result of pulling to fast. Interestingly, in the process of calculating the local GC fraction from the sequence, the sequence had to be reversed in order for the histogram peaks of the backward data to match the troughs of the local GC fraction and to match the pattern seen in Heinsman (2017).

In the same fashion as the overstretching model, the unzipping equilibrium model can be used in experimental situations due to its simplicity and ease of use. Preferably, it is to be used on equilibrium data, but it has proven to be useful in obtaining upper and lower bounds to the equilibrium values of the model parameters.

5.4   Conclusion

The covalent DNA tethering protocol cannot be used for chromatin yet to create a practical amount of long-lifetime tethers. When preparing synthetic nucleosomes, a large part of the tethers will not contain a nucleosome (Dyer et al., 2003). The high yield obtained in the original work (Gidi et al., 2018) shows that there is much to gain, facilitating long-lifetime chromatin tethers in the future.

The equilibrium models that were developed for overstretching and unzipping were successful. The design of these models can be further exploited in more advanced models.

Such models could contain extra states such as nucleosome energy barriers.

The force barrier localization methods that were developed can be used on nucleosomes in the future to determine their location along the sequence. Similar methods have proven to be vital in the unzipping of single synthetic nucleosomes using optical tweezers (Shundrovsky et al., 2006; Hall et al., 2009; Li and Wang, 2012). The techniques could be especially useful for native chromatin. This will show if similar strong interaction regions are found along native nucleosomes as well. This will contribute to the knowledge of how nucleosomes play a role in gene expression.

Acknowledgements

Bibliography

Backer, A. S., Biebricher, A. S., King, G. A., Wuite, G. J. L., Heller, I., and Peterman, E. J. G. (2019). Single-molecule polarization microscopy of DNA intercalators sheds light on the structure of S-DNA. *Science Advances*, 5(3).

Bintu, L., Ishibashi, T., Dangkulwanich, M., Wu, Y.-Y., Lubkowska, L., Kashlev, M., and Bustamante, C. (2012). Nucleosomal Elements that Control the Topography of the Barrier to Transcription. *Cell*, 151(4):738–749.

Bockelmann, U., Essevaz-Roulet, B., and Heslot, F. (1997). Molecular Stick-Slip Motion Revealed by Opening DNA with Piconewton Forces. *Phys. Rev. Lett.*, 79(22):4489–4492.

Bongini, L., Lombardi, V., and Bianco, P. (2014). The transition mechanism of DNA overstretching: a microscopic view using molecular dynamics. *Journal of The Royal Society Interface*, 11(97):20140399.

Bosco, A., Camunas-Soler, J., and Ritort, F. (2013). Elastic properties and secondary structure formation of single-stranded DNA at monovalent and divalent salt conditions. *Nucleic Acids Research*, 42(3):2064–2074.

Brouwer, T. B., Hermans, N., and van Noort, J. (2020). Multiplexed Nanometric 3D Tracking of Microbeads Using an FFT-Phasor Algorithm. *Biophysical Journal*, 118(9):2245–2257.

Brouwer, T. B., Kaczmarczyk, A., Pham, C., and van Noort, J. (2018). *Unraveling DNA Organization with Single-Molecule Force Spectroscopy Using Magnetic Tweezers*, pages 317–349. Springer New York, New York, NY.

Chen, Z., Gabizon, R., Brown, A. I., Lee, A., Song, A., Díaz-Celis, C., Kaplan, C. D., Koslover, E. F., Yao, T., and Bustamante, C. (2019). High-resolution and high-accuracy topographic and transcriptional maps of the nucleosome barrier. *eLife*, 8:e48281.

Cluzel, P., Lebrun, A., Heller, C., Lavery, R., Viovy, J.-L., Chatenay, D., and Caron, F. (1996). DNA: An Extensible Molecule. *Science*, 271(5250):792–794.

de Odrowaz Piramowicz, M., Czuba, P., Targosz, M., Burda, K., and Szymoński, M. (2006). Dynamic force measurements of avidin-biotin and streptavdin-biotin interactions using AFM. *Acta Biochimica Polonica*, 53(1):93–100.

De Vlaminck, I., Henighan, T., van Loenhout, M. T. J., Burnham, D. R., and Dekker, C. (2012). Magnetic Forces and DNA Mechanics in Multiplexed Magnetic Tweezers. *PLOS ONE*, 7(8):1–10.

Dyer, P. N., Edayathumangalam, R. S., White, C. L., Bao, Y., Chakravarthy, S., Muthurajan, U. M., and Luger, K. (2003). Reconstitution of Nucleosome Core Particles from Recombinant Histones and DNA. In *Chromatin and Chromatin Remodeling Enzymes, Part A*, volume 375 of *Methods in Enzymology*, pages 23 – 44. Academic Press.

Eeftens, J. M., van der Torre, J., Burnham, D. R., and Dekker, C. (2015). Copper-free click chemistry for attachment of biomolecules in magnetic tweezers. *BMC Biophysics*, 8:9.

Gidi, Y., Bayram, S., Ablenas, C. J., Blum, A. S., and Cosa, G. (2018). Efficient One-Step PEG-Silane Passivation of Glass Surfaces for Single-Molecule Fluorescence Studies. *ACS Applied Materials & Interfaces*, 10(46):39505–39511.

Hall, M. A., Shundrovsky, A., Bai, L., Fulbright, R. M., Lis, J. T., and Wang, M. D. (2009). High-resolution dynamic mapping of histone-DNA interactions in a nucleosome. *Nature Structural & Molecular Biology*, 16:124–129.

Heinsman, J. (2017). Magnetic tweezers experiments in low salt conditions and unzipping of double stranded DNA. Master's thesis, Leiden University, Leiden, The Netherlands.

Hermans, N., Huisman, J. J., Brouwer, T. B., Schächner, C., van Heusden, G. P. H., Griesenbeck, J., and van Noort, J. (2017). Toehold-enhanced LNA probes for selective pull down and single-molecule analysis of native chromatin. *Scientific Reports*, 7:16721.

Hodges, C., Bintu, L., Lubkowska, L., Kashlev, M., and Bustamante, C. (2009). Nucleosomal Fluctuations Govern the Transcription Dynamics of RNA Polymerase II. *Science*, 325(5940):626–628.

Janissen, R., Berghuis, B. A., Dulin, D., Wink, M., van Laar, T., and Dekker, N. H. (2014). Invincible DNA tethers: covalent DNA anchoring for enhanced temporal and force stability in magnetic tweezers experiments. *Nucleic Acids Research*, 42(18):e137–e137.

Kaczmarczyk, A. (2019). *Nucleosome stacking in chromatin fibers probed with single-molecule force- and torque-spectroscopy*. PhD thesis, Leiden University, Leiden, The Netherlands.

Kaczmarczyk, A., Meng, H., Ordu, O., van Noort, J., and Dekker, N. H. (2020). Chromatin fibers stabilize nucleosomes under torsional stress. *Nature Communications*, 11(126).

King, G. A., Gross, P., Bockelmann, U., Modesti, M., Wuite, G. J. L., and Peterman, E. J. G. (2013). Revealing the competition between peeled ssDNA, melting bubbles, and S-DNA during DNA overstretching using fluorescence microscopy. *Proceedings of the National Academy of Sciences*.

Li, M. and Wang, M. D. (2012). Unzipping single DNA molecules to study nucleosome structure and dynamics. *Methods in Enzymology*, 513:29–58.

Li, N., Wang, J., Ma, K., Liang, L., Mi, L., Huang, W., Ma, X., Wang, Z., Zheng, W., Xu, L., Chen, J.-H., and Yu, Z. (2019). The dynamics of forming a triplex in an artificial telomere inferred by DNA mechanics. *Nucleic Acids Research*, 47(15):e86–e86.

Marko, J. F. and Neukirch, S. (2013). Global force-torque phase diagram for the dna double helix: Structural transitions, triple points, and collapsed plectonemes. *Phys. Rev. E*, 88(6):062722.

Meng, H., Andresen, K., and van Noort, J. (2015). Quantitative analysis of single-molecule force spectroscopy on folded chromatin fibers. *Nucleic Acids Research*, 43(7):3578–3590.

Neuert, G., Albrecht, C., Pamir, E., and Gaub, H. E. (2006). Dynamic force spectroscopy of the digoxigenin–antibody complex. *FEBS Letters*, 580:505–509.

Odijk, T. (1995). Stiff Chains and Filaments under Tension. *Macromolecules*, 28(20):7016–7018.

SantaLucia, J. (1998). A unified view of polymer, dumbbell, and oligonucleotide DNA nearest-neighbor thermodynamics. *Proceedings of the National Academy of Sciences*, 95(4):1460–1465.

Shundrovsky, A., Smith, C. L., Lis, J. T., Peterson, C. L., and Wang, M. D. (2006). Probing SWI/SNF remodeling of the nucleosome by unzipping single DNA molecules. *Nature Structural & Molecular Biology*, 13:549–554.

Smith, S. B., Cui, Y., and Bustamante, C. (1996). Overstretching B-DNA: The Elastic Response of Individual Double-Stranded and Single-Stranded DNA Molecules. *Science*, 271(5250):795–799.

Vendel, K. (2015). The role of the linker histone in chromatin structure and dynamics. Master's thesis, Leiden University, Leiden, The Netherlands.

Walsh, M. K., Wang, X., and Weimer, B. C. (2001). Optimizing the immobilization of single-stranded DNA onto glass beads. *Journal of Biochemical and Biophysical Methods*, 47(3):221 – 231.

Yu, Z., Dulin, D., Cnossen, J., Köber, M., van Oene, M. M., Ordu, O., Berghuis, B. A., Hensgens, T., Lipfert, J., and Dekker, N. H. (2014). A force calibration standard for magnetic tweezers. *Review of Scientific Instruments*, 85(12):123114.

Zhang, X., Chen, H., Fu, H., Doyle, P. S., and Yan, J. (2012). Two distinct overstretched DNA structures revealed by single-molecule thermodynamics measurements. *Proceedings of the National Academy of Sciences*, 109(21):8103–8108.